

Leptophilic Effective WIMPs

Spencer Chang*, Ralph Edezhath†, Jeffrey Hutchinson†, and Markus Luty†

**Institute of Theoretical Science, University of Oregon
Eugene, Oregon 97403*

*†Physics Department, University of California, Davis
Davis, California 95616*

Abstract

Effective WIMP models are minimal extensions of the standard model that explain the relic density of dark matter by the “WIMP miracle.” In this paper we consider the phenomenology of effective WIMPs with trilinear couplings to leptons and a new “lepton partner” particle. The observed relic abundance fixes the strength of the cubic coupling, so the parameters of the models are defined by the masses of the WIMP and lepton partner particles. This gives a simple parameter space where collider and direct detection experiments can be compared under well-defined physical minimality assumptions. The most sensitive collider probe is the search for leptons + MET, while the most sensitive direct detection channel is scattering from nuclei arising from loop diagrams. Collider and direct detection searches are highly complementary: colliders give the only meaningful constraint when dark matter is its own antiparticle, while direct detection is generally more sensitive if the dark matter is not its own antiparticle.

1 Introduction

The observation of dark matter is an unambiguous discovery of physics beyond the standard model. The simplest and most compelling explanation for dark matter is a stable thermal relic, a weakly interacting massive particle (WIMP). Assuming that it freezes out by annihilation to standard model particles via dimensionless order-1 couplings, the correct relic density is obtained for dark matter masses of order 100 GeV to 1 TeV. This “WIMP miracle” means that dark matter can potentially be directly produced and studied at high-energy collider experiments such as the LHC. At the same time, this coupling allows for direct detection of astrophysical dark matter through its interactions with ordinary matter. It is one of the most ambitious dreams of particle physics to be able to discover dark matter in both types of experiment, and make a direct comparison to properties of dark matter inferred from cosmology and astrophysics.

There are many well-motivated models of physics beyond the standard model that have a WIMP candidate (for example, the minimal supersymmetric standard model), but comparing collider and direct detection sensitivity is generally model-dependent due to the large number of independent parameters in these theories. In a previous paper [1], we proposed a class of minimal models where it is assumed that the only particles beyond the standard model that are important for dark matter phenomenology consist of the WIMP and a standard model “partner” particle with the same gauge quantum numbers as one of the standard model particles. This allows a cubic coupling of the form

$$\Delta\mathcal{L} \sim \lambda(\text{SM})(\widetilde{\text{SM}})(\text{DM}), \quad (1.1)$$

where DM denotes the dark matter particle and SM ($\widetilde{\text{SM}}$) denote the standard model field and its partner, respectively. The coupling λ is fixed by requiring the correct relic abundance, so the only parameters in this model are the masses of the WIMP and the standard model partner particle, once the spin and CP properties of the dark matter is fixed. This gives a well-defined and complete effective theory for dark matter phenomenology, motivating the name “effective WIMP” for this class of models. In particular, it allows direct comparison of the collider and direct detection searches for dark matter under well-defined physical minimality assumptions.

Ref. [1] analyzed the phenomenology in the case where the standard model particle and its partner are colored. In this case collider and direct detection experiments were found to be highly complementary. Similar models were also studied in Refs. [2–5]. The major difference in our work is that we focus on the parameter space where the WIMP has the correct thermal relic abundance. This has important implications for

the global picture. For example, Ref. [1] found that the coupling λ is enhanced in some regions of parameter space, leading to increased sensitivity for collider and direct detection searches. On the other hand, the relic abundance constraint eliminates regions of parameter space where indirect detection limits are important. There has also been other approaches to simplified dark matter such as s -channel mediators [6–8] and dark matter with electroweak interactions [9, 10].

In this paper, we consider effective WIMP models where the standard model particle is a lepton (e, μ, τ or their corresponding neutrinos). In this case, the collider constraints come from the pair production of lepton partners followed by their decay into a WIMP plus a lepton or neutrino, and so the collider constraints are independent of the value of λ . Once again, we find that collider and direct detection experiments are highly complementary. The direct detection constraints depend on λ , with the dominant interactions coming from loop diagrams to a photon. The type of interactions allowed depend on whether the dark matter is its own antiparticle, which strongly affects the scattering rate. If the dark matter is its own antiparticle, the only meaningful constraints come from collider experiments, while in the opposite case direct detection experiments are generally more sensitive. There is a significant region of parameter space where both future collider and direct detection experiments can see a signal.

Imposing the relic abundance constraints has an important effect on the direct detection phenomenology. In particular, these constraints extend into the regime of large lepton partner masses because the coupling λ becomes large in this region to get the correct relic abundance. Imposing the relic abundance constraint also implies that constraints from indirect detection are not important.

The models that we consider are listed in Table 1. We consider couplings to left-handed lepton doublets only, since the phenomenology of right-handed leptons is essentially a subset of this case. Note that this fixes the production rate at colliders which leads to slightly stronger constraints than the right-handed lepton partner case. We consider both the cases where the dark matter couples to only the first two generations of leptons, as well as the case where it couples to all generations. We find that the differences between them are small, as one might expect.

Particles		\mathcal{L}_{int}
Dark matter χ	Lepton partner L	
Majorana fermion	Complex scalar	$\lambda(\chi\ell)L^* + \text{h.c.}$
Dirac fermion	Complex scalar	$\lambda(\chi\ell)L^* + \text{h.c.}$
Real scalar	Dirac fermion	$\lambda(L^c\ell)\chi + \text{h.c.}$
Complex scalar	Dirac fermion	$\lambda(L^c\ell)\chi + \text{h.c.}$

Table 1. Summary of the models considered in this paper. Spinors are written in 2-component notation. Here ℓ is the left-handed lepton doublet of the standard model, L is the lepton partner field, and χ is the dark matter field.

2 General Features

2.1 Relic Abundance

The relic abundance of non-baryonic matter is accurately determined by cosmological constraints to be $\Omega_\chi h^2 = 0.1199 \pm 0.0027$ [11]. We assume that the dark matter is entirely composed of the WIMP in our model, denoted henceforth by χ . Under the assumption that χ particles were in thermal equilibrium in the early universe, its present relic density is determined by freeze-out from the annihilation process $\chi\bar{\chi} \rightarrow \ell\bar{\ell}$ shown in Fig. 1. The relic abundance is determined by the thermally averaged annihilation cross section $\langle\sigma(\chi\bar{\chi} \rightarrow \ell\bar{\ell})v\rangle$ at temperatures $T_f \sim m_\chi/25$. The dark matter velocity during annihilation is $v^2 \sim 0.1$, so we can expand

$$\sigma(\chi\bar{\chi} \rightarrow \ell\bar{\ell})v = a + bv^2 + O(v^4). \quad (2.1)$$

Approximate formulas for the relic density in terms of these parameters are given in Appendix A. The coefficients a and b represent s -wave and p -wave contributions, and are computed in each model below.

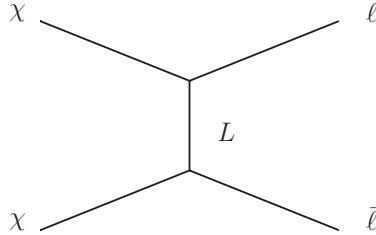


Fig. 1. Feynman diagram contributing to dark matter freeze-out

2.2 Collider Limits

The dark matter can be produced at colliders by Drell-Yan production via an intermediate W , Z , or γ . The relic abundance constraint means that the coupling λ is always sufficiently large that the lepton partner decays promptly. The collider phenomenology is therefore independent of λ , and depends only on the masses and the spin of the new particles. The charged lepton partners decay to $\ell\chi$, while the neutral lepton partners decay invisibly to $\nu\chi$, so there are signal events with 0, 1, or 2 charged leptons. This paper focuses on the dilepton channel, but we make some brief remarks about the other channels below.

The totally invisible channel can be probed by monojet searches, but requiring a jet from initial state radiation leads to a small rate with weak constraints. The 1 lepton + MET channel has been searched for in the context of W' models [12]. We have checked that the event rates for lepton partner production are too small to provide the most important collider constraints in this channel, even in the case of fermionic lepton partners which have the largest rate.

We therefore turn to the dilepton plus MET channel. This has been searched for by both ATLAS [13] and CMS [14], which very helpfully have cross section limits as a function of the particle masses. We use the most recent ATLAS results for this paper. The event rates were calculated at parton level using **MadGraph5** v1.5.11 [15]. The **MadGraph** model files were generated using **FeynRules** v1.6.0 [16].

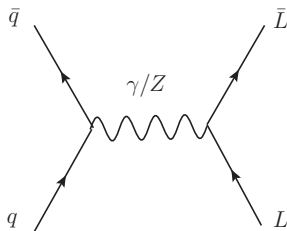


Fig. 2. Feynman diagram contributing to leptons + MET signal at colliders.

The ATLAS search was for sleptons, which have a lower cross section than fermionic lepton partners with the same mass. They report limits on $\sigma \times \text{BR}$ only for slepton masses up to ~ 350 GeV and dark matter masses up to ~ 200 GeV, but their search should be sensitive to fermionic lepton partners beyond this range. We extrapolate the ATLAS search in the following way. The maximum allowed $\sigma \times \text{BR}$ is expected to depend mainly on $m_L - m_\chi$, which controls the p_T of the lepton and the MET. The bound gets weaker for small values of $m_L - m_\chi$, so we fitted the reported ATLAS

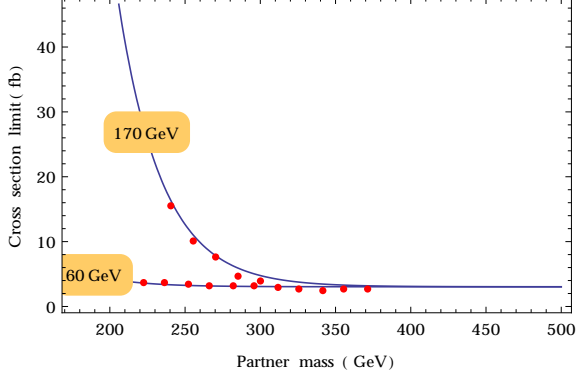


Fig. 3. Extrapolation of limits for 2 lepton + MET search as a function of m_L for fixed m_χ , compared with ATLAS reported limits.

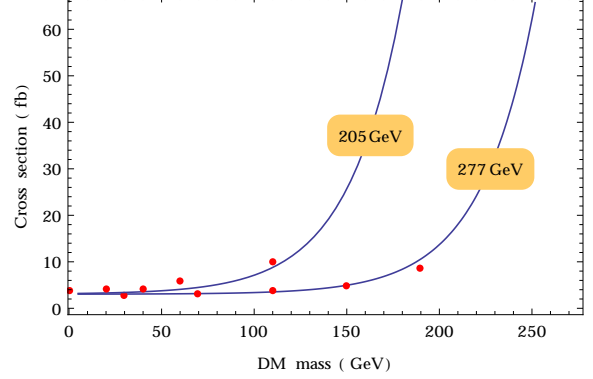


Fig. 4. Extrapolation of limits for 2 lepton + MET search as a function of m_χ for fixed m_L , compared with ATLAS reported limits.

results to the function

$$(\sigma \times \text{BR})_{\text{limit}} = a + be^{-c(m_L - m_\chi)}. \quad (2.2)$$

This works well over the range reported by ATLAS, as can be seen in Figs. 3 and 4. The CMS search has limits for a larger mass range, but we find it has weaker limits than the extrapolated ATLAS limits, so we use the latter in our plots.

2.3 Direct Detection

For dark matter interacting with leptons, there are important modifications to the sensitivity of direct detection experiments. To couple to the nucleus, interactions occur at loop level through induced electromagnetic form factors of the dark matter [17], such as a charge radius or magnetic moment. There have also been analyses of the possibility of detecting dark matter scattering from electrons in the atoms [18–20] with a published limit using XENON10 data [21]. However, these processes are more important for dark matter masses below a GeV, where the dark matter has insufficient kinetic energy to give detectable ($\sim \text{keV}$) nuclear recoil energies.

In this paper, we focus on dark matter heavier than a GeV, so from now on we will consider only scattering with the nucleus. The leading WIMP-nucleus interactions arise at 1-loop level through diagrams of the form Fig. 5. This gives rise to interactions to the photon through a charge radius operator

$$\mathcal{L}_{\text{charge radius}} = \begin{cases} 2b_\chi \partial_\mu \chi^* \partial_\nu \chi F^{\mu\nu} & (\text{complex scalar DM}) \\ b_\chi \bar{\chi} \gamma_\nu \chi \partial_\mu F^{\mu\nu} & (\text{Dirac fermion DM}) \end{cases} \quad (2.3)$$

and a magnetic moment operator for the Dirac fermion

$$\mathcal{L}_{\text{magnetic moment}} = \frac{\mu_\chi}{2} \bar{\chi}^* \sigma_{\mu\nu} \chi F^{\mu\nu} \text{ (Dirac fermion DM)}. \quad (2.4)$$

See sections A.1 and A.2 in the appendix for detailed results of our calculation of these coefficients. As a check, we confirmed that our formulas agree for the Dirac fermion case with [22, 23] in the relevant limits. Of the two contributions to the scattering of a Dirac fermion, the charge radius is typically larger because the charged radius strength has a logarithmic enhancing factor of $\ln(m_L^2/m_\ell^2) \sim 10$. The scattering cross section from this operator is given by

$$\frac{d\sigma_{b_\chi}}{dE_R} = \frac{m_N}{2\pi v^2} Z^2 e^2 b_\chi^2 F^2[E_R] \quad (2.5)$$

where $F[E_R]$ is the nucleus charge form factor. This is a spin-independent interaction, so we use the current best limits from LUX's 85.3 day run [24]. We also use projected sensitivities for XENON1T taken from **DMtools** [25].

When the dark matter is its own antiparticle, symmetry requires the charge radius and magnetic moment to vanish. For real scalar dark matter, there is no magnetic moment because it is spin-0, and the charge radius operator vanishes due to anti-symmetry of the field strength tensor. Therefore there is no 1-loop contribution in this case. The leading interaction with nuclei arises from 2-loop interactions such as the one shown in Fig. 6. The additional suppression reduces the WIMP-nucleus cross section to well below current limits.

For Majorana dark matter, the vector and tensor operator are zero, so the dipole moment and the charge radius vanish. The leading interaction comes from an anapole moment operator of the form

$$\bar{\chi} \gamma_5 \gamma_\mu \chi \partial_\nu F^{\mu\nu}, \quad (2.6)$$

which also leads to a cross section below direct detection limits, except for the case where the dark matter and lepton partner are extremely degenerate, as discussed recently in [26]. See §A.3 and A.4 in the appendix for more details on the direct detection for Majorana and real scalar dark matter.

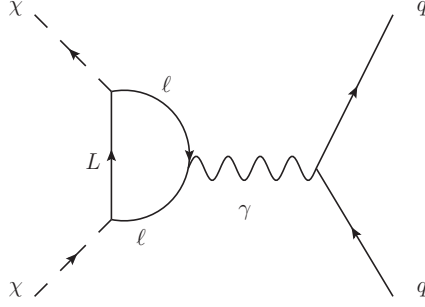


Fig. 5. Schematic 1-loop contributions for direct detection. There are also diagrams where the lepton-partner (L) and lepton (ℓ) are interchanged.

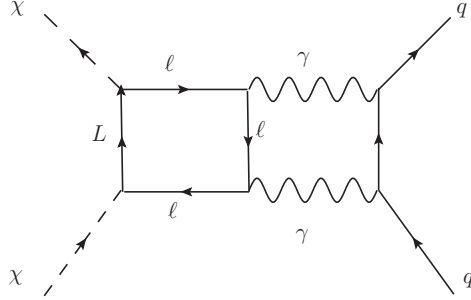


Fig. 6. Schematic 2-loop contributions to direct detection scattering. There are also diagrams where the lepton-partner (L) and lepton (ℓ) are interchanged and where the photons are crossed.

As will be shown later, direct detection experiments provide the most stringent limits for Dirac fermion or complex scalar dark matter. These limits extend to extremely high masses in two regions of parameter space: near $m_L \sim m_\chi$ and $m_L \gg m_\chi$. In the first region the particles are nearly degenerate, and there is an enhancement due to the possibility of the virtual partner particle going (nearly) on-shell in Fig. 5. This can be seen in the charge radius Eq. (A.5) which diverges in the limit $m_\chi \rightarrow m_L$. On the other hand, for the $m_L \gg m_\chi$ region, the direct detection constraint remains strong because the coupling λ is required to become larger to obtain the observed relic abundance. Fixing the dark matter mass, the annihilation cross section requires the interaction strength to scale as

$$\lambda^4 \sim 4\pi\sigma_{\text{ann}} \frac{m_L^4}{m_\chi^2}. \quad (2.7)$$

Model		Relic Abundance	Direct Detection
χ	L		
Majorana fermion	Complex scalar	$a \sim m_\ell^2$ $\lambda \sim 0.5 - 3$	Anapole Scattering
Dirac fermion	Complex scalar	$\lambda \sim 0.2 - 1$	One loop charge radius $\sigma_{\text{SI}} \stackrel{m_L \gg m_\chi}{\sim} \frac{m_p^2}{m_\chi^2} \sigma_{\text{ann}}$
Real scalar	Dirac fermion	$a, b \sim m_\ell^2$ $\lambda \sim 1 - 7$	Two loop scattering through two photons
Complex scalar	Dirac fermion	$a \sim m_\ell^2$ $\lambda \sim 0.5 - 3$	One loop charge radius $\sigma_{\text{SI}} \stackrel{m_L \gg m_\chi}{\sim} \frac{m_p^2}{m_\chi^2} \sigma_{\text{ann}}$

Table 2. Overview of results for relic abundance and direct detection for the various models.

At large m_L , the charge radius is given by

$$b_\chi \sim \frac{\lambda^2 e}{16\pi^2 m_L^2} \left[1 + \frac{2}{3} \ln \frac{m_\ell^2}{m_L^2} \right] \sim \frac{e\sqrt{4\pi\sigma_{\text{ann}}}}{16\pi^2 m_\chi} \left[1 + \frac{2}{3} \ln \frac{m_\ell^2}{m_L^2} \right] \quad (2.8)$$

Thus, aside from the logarithm, the increase in m_L does not change the charge radius or the scattering cross section, leading to an asymptotic limit on m_χ .

2.4 Indirect Detection

In these models, the dark matter in our galaxy will annihilate into charged leptons and neutrinos with a cross section bounded by that required by the relic abundance. So all of these annihilation cross sections are bounded $\langle \sigma(\chi\bar{\chi} \rightarrow \bar{\ell}\ell)v \rangle \leq 3 \times 10^{-26} \text{ cm}^3/\text{s}$. The only indirect detection constraints that are sensitive to such a cross section is annihilation into tau leptons. These are constrained by the resultant gamma ray production from the tau decays that could have been seen by Fermi observations of Milky Way satellites [27, 28]. These set an upper limit on the dark matter mass, which is sensitive to systematic uncertainties of the dark matter distribution of these objects. The analysis [27] shows that this uncertainty allows the limit to range from $m_\chi < 13 - 80 \text{ GeV}$. So there is a limit for models coupling to the third generation leptons but there are significant uncertainties, so we choose to omit it from our later plots.

2.5 Muon Anomalous Magnetic Moment

The anomalous magnetic moment of the muon a_μ receives corrections from loops of χ and L particles in our models. There is nominally a $\sim 3\sigma$ discrepancy between the measured value of a_μ and the value predicted in the standard model (for a review, see [29]). However, there are large theoretical uncertainties, particular in the light-by-light scattering which can only be estimated from strong interaction models [29]. Our point of view is that corrections to a_μ that make the discrepancy significantly worse can be used to constrain new physics, but we do not believe that regions that reduce the discrepancy are favored.

The contributions to the photon-muon-muon amplitude are parameterized as

$$\mathcal{M} = ie\bar{u} \left(\gamma^\lambda + (a_\mu^{SM} + \delta a_\mu) \frac{i\sigma^{\lambda\beta} q_\beta}{2m_\mu} \right) u \epsilon_\lambda \quad (2.9)$$

We can read off the contributions from the calculations in supersymmetric models, computed in Ref. [30]. For fermionic dark matter, χ is identified as a neutralino, and L is identified as a slepton, and we obtain

$$\delta a_{\mu,fermion} = -\frac{\lambda^2 m_\mu^2}{192\pi^2 m_L^2} \frac{2}{(1-r_L)^4} (1 - 6r_L + 3r_L^2 + 2r_L^3 - 6r_L \ln(r_L)) \quad (2.10)$$

where $r_L = m_\chi^2/m_L^2$. Note that this contribution is in the opposite direction of the observed discrepancy. For scalar dark matter, χ is identified as a sneutrino, and L is identified as a chargino, and we obtain

$$\delta a_{\mu,scalar} = \frac{\lambda^2 m_\mu^2}{192\pi^2 m_\chi^2} \frac{2}{(1-r_L^{-1})^4} (2 + 3r_L^{-1} - 6r_L^{-2} + r_L^{-3} - 6r_L^{-1} \ln(r_L)) \quad (2.11)$$

This contribution is in the same sign as the observed discrepancy. For both scalar and fermion dark matter, these contributions are comparable to the observed discrepancy only for very light dark matter, $\lesssim 10$ GeV. We focus on heavier dark matter, and therefore do not consider these constraints when presenting our results.

3 Results

3.1 Dirac Dark Matter

The collider and direct detection constraints for Dirac dark matter are shown in Fig. 7 for the coupling to the first two generations of leptons, and in Fig. 8 for the coupling to all three generations. The results of these two cases are very similar, and

probably within the errors of the bounds. A collider limit on τ partners would give an additional probe of the model that couples to all generations of leptons.

The dominant direct detection constraint comes from WIMP-nucleus scattering. The contribution from the charge radius operator Eq. (2.5) dominates over the contribution from the dipole operator Eq. (A.9). This is a spin-independent interaction, so we use the limits from LUX. The LUX limits are strong in the degenerate region $m_\chi \simeq m_L$. But this is also the region where co-annihilation effects are important, so our results are not reliable. As discussed earlier, at large m_L there is an asymptotic limit on m_χ due to the increase in the interaction strength as mandated by the relic abundance constraint. Although we focus on heavy dark matter, we note that dark matter masses below approximately 8 GeV are not ruled out by LUX because the smaller energy deposit results in reduced sensitivity and there should then be an allowed region for LUX at light enough dark matter mass.

The projected limits for XENON1T extend to dark matter masses up to approximately 650 GeV, covering essentially the entire parameter space shown in Figs. 7 and 8. Thus, if XENON1T sees no excess, then we should not expect to see any lepton partner signals in the next run of the LHC. However, there is still a large viable region around the elbow of the LUX limit where we could have future correlated signals at XENON1T and LHC.

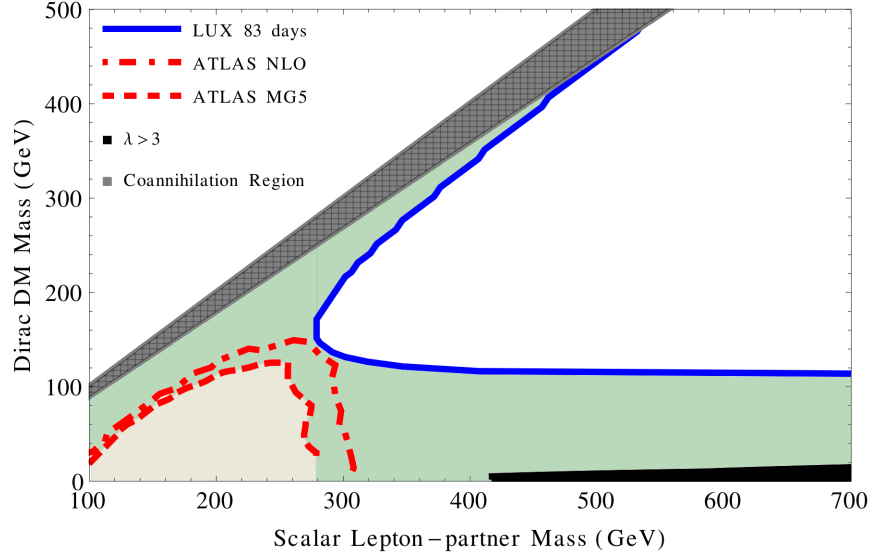


Fig. 7. Limits on Dirac dark matter coupling to first 2 generations of leptons only.

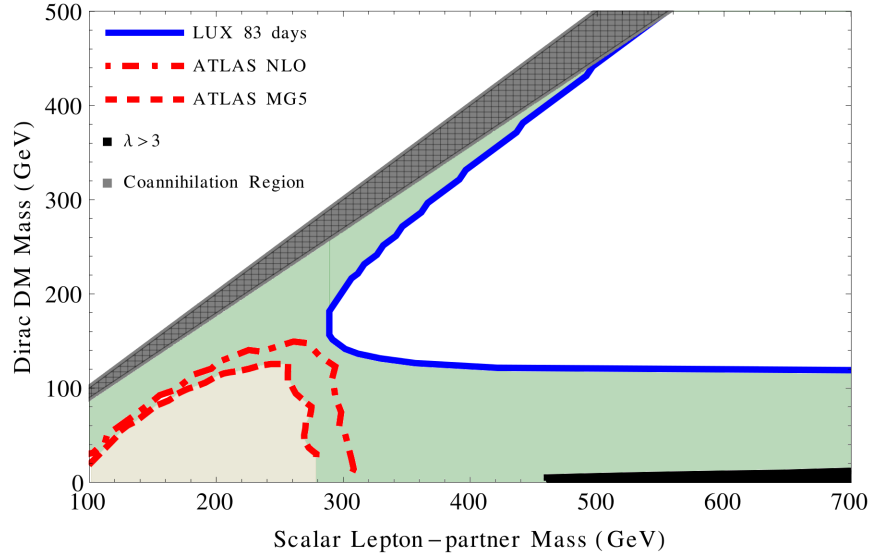


Fig. 8. Limits on Dirac dark matter coupling to all 3 generations of leptons.

3.2 Complex Scalar Dark Matter

The collider and direct detection constraints for complex scalar dark matter are shown in Fig. 9 for the coupling to the first two generations of leptons, and in Fig. 10 for the coupling to all three generations. The results of these two cases are very similar, and probably within the errors of the bounds. The collider limits are stronger than for scalar lepton partners because of the larger production cross section. As discussed in the main text, the ATLAS dilepton search does not report bounds for the full range of sensitivity. We show both the reported and extrapolated bounds and it is clear that there should be sensitivity to higher partner masses. In fact, our extrapolation shows that it could be stronger than the LUX direct detection bounds.

As in the Dirac dark matter case, the LUX bounds are strong both in the degenerate region and the region of large m_L . Again, dark matter masses below 8 GeV are not constrained. The projected XENON1T sensitivity covers the entire parameter space shown in Figs. 9 and 10, and extend up to dark matter masses of approximately 1 TeV. Once more there is viable parameter space which will be covered by future LHC data and direct detection experiments.

This model can account for the observed discrepancy in the muon anomalous moment for $2.2 \text{ GeV} < m_\chi < 7.3 \text{ GeV}$ for dark matter coupling to the first 2 generations of leptons, and $1.8 \text{ GeV} < m_\chi < 5.0 \text{ GeV}$ for coupling to all 3 generations of leptons. Given the theoretical uncertainties in the standard model prediction for the

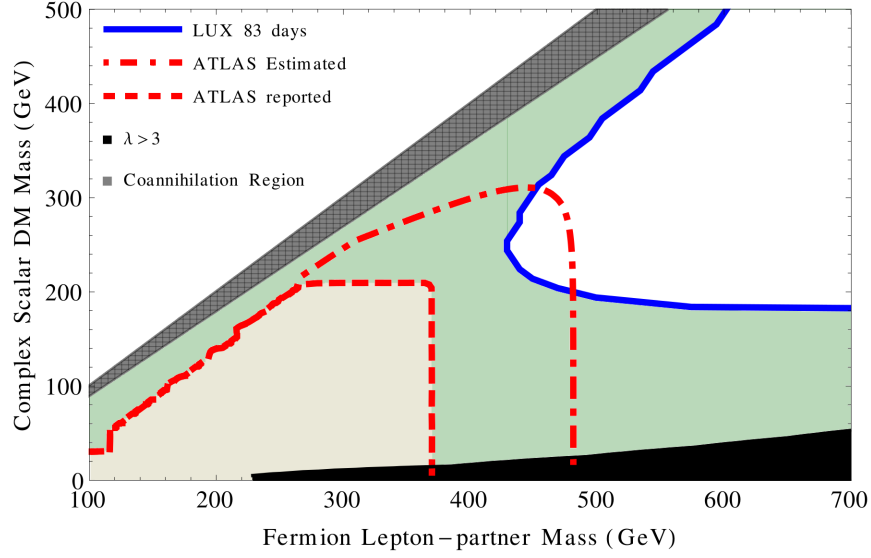


Fig. 9. Limits on complex scalar dark matter coupling to first 2 generations of leptons.

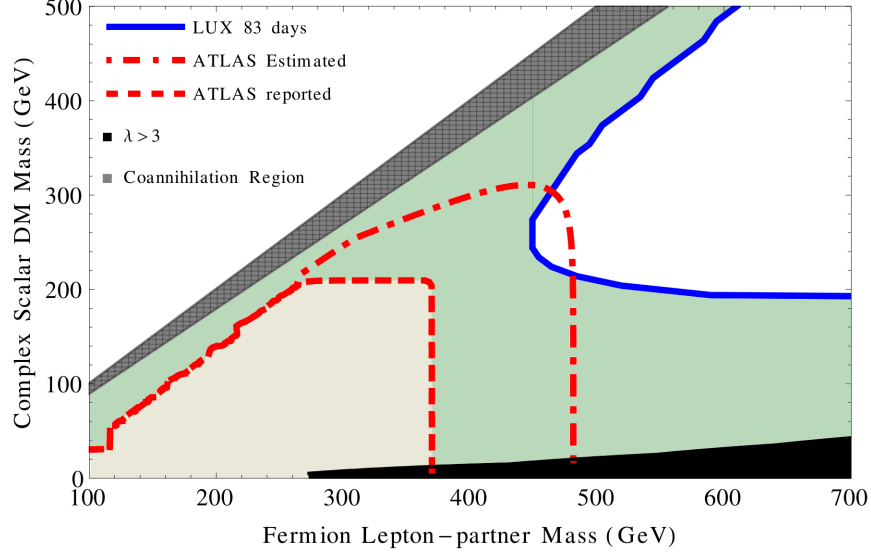


Fig. 10. Limits on complex scalar dark matter coupling to all 3 generations of leptons.

anomalous magnetic moment, we do not believe this region of parameters is strongly preferred, but it is intriguing that this is the region where the direct detection constraints are weak. However, to be consistent with the ATLAS search pushes one to the strong coupling region at larger m_L where $\lambda > 3$ and thus these leading order results are not expected to be reliable.

3.3 Real Scalar and Majorana Dark Matter

The collider bounds for the real scalar (Majorana) dark matter are identical to the bounds for complex scalar (Dirac) dark matter. This is because the only production mechanism is via the coupling to a photon or Z , so the bounds are independent of the coupling λ .

The dominant direct detection cross section arises from 2-loop diagrams contributing to WIMP-nucleus scattering, and these are orders of magnitude below current and projected experimental limits. Following the discussion in [26], Majorana dark matter has an anapole moment which normalized to the Bohr magneton is $\frac{A}{\mu_N} \sim 10^{-6}$ fm or smaller in the thermal relic parameter space. As inferred in [26], the LUX limits are sensitive to values $\sim 10^{-5}$ fm or higher. Even with projected XENON1T sensitivity, we find that this will not place limits on this model either. For real scalar dark matter, the direct detection must go through two photons as shown in Fig. 6, which leads to an extremely suppressed cross section below 10^{-53} cm², which will never be reached by any future experiment.

4 Conclusions

We have considered minimal extensions of the standard model containing electroweak singlet dark matter with renormalizable couplings to leptons and lepton “partner” particles. These models naturally explain the observed relic abundance of dark matter by the “WIMP miracle.” The strength of the coupling is fixed by requiring the correct relic abundance, so these models are parameterized only by the masses of the dark matter and the lepton partner particles. This gives a simple model where direct detection and dark matter searches at colliders can be compared under well-defined physical minimality assumptions.

Previous studies focused on effective WIMPs coupled to colored standard model particles, while this paper focuses on effective WIMPs coupled to leptons. As in the previous case, we find that collider and direct detection experiments are remarkably complementary. The collider limits depend only on the spin and masses of the particles, and not whether dark matter is its own antiparticle. The dominant constraint comes from the dilepton plus MET channel. We find that the mono-lepton channel is less sensitive in these models.

Direct detection experiments place interesting bounds only in the case where the dark matter is not its own anti-particle, *i.e.* Dirac or complex scalar dark matter. In these cases, current direct detection limits are generally stronger than collider limits,

although there is an interesting region near $m_\chi \sim m_L/2$, where collider limits are competitive or stronger. In this region, it is possible to discover the dark matter in both future collider and direct detection experiments. In particular, the next generation of direct detection experiments (e.g. XENON1T) will be sensitive to the bulk of parameter space.

However, if the dark matter is its own antiparticle (*i.e.* Majorana or real scalar dark matter) the direct detection bounds are well below the reach of current and next generation experiments, while the collider bounds are unaffected. In this case, leptophilic effective WIMPs can be discovered only in collider experiments.

Note: As this work was being completed Ref. [31] appeared, which analyzes the same models without the relic abundance constraint and makes projections for lepton partner reaches at the 14 TeV LHC.

Acknowledgements

SC would like to thank Graham Kribs and Yang Bai for discussions. SC was supported in part by the Department of Energy under grant DE-SC0009945. RE, JH, and ML were supported in part by the Department of Energy under grant DE-FG02-91ER40674.

Appendix A: Model Details

A.1 Dirac Dark Matter

Relic Density: The relic density is determined by the velocity-averaged annihilation cross section $\langle\sigma v\rangle$ which is commonly parametrized by the coefficients

$$\langle\sigma v\rangle \simeq a + bv^2$$

In this model, for the annihilation cross section $\chi\chi^\dagger \rightarrow \ell\ell^\dagger$, a and b are found to be

$$a = \frac{m_\chi^2 \sqrt{1-r} \lambda^4}{32\pi (m_L^2 - m_\chi^2(r-1))^2} \quad (\text{A.1})$$

$$b = \frac{\lambda^4 m_\chi^2}{768\pi (m_L^2 - m_\chi^2(r-1))^4 \sqrt{1-r}} \left[m_L^4 (8 - 7r + 2r^2) + m_\chi^4 (r-1)^2 (-8 + 9r + 2r^2) + 2m_L^2 m_\chi^2 (-12 + 13r + r^2 - 2r^3) \right] \quad (\text{A.2})$$

To lowest order in $r = m_l^2/m_\chi^2$,

$$a \stackrel{r \rightarrow 0}{\simeq} \frac{\lambda^4 m_\chi^2}{32\pi (m_L^2 + m_\chi^2)^2} \quad (\text{A.3})$$

$$b \stackrel{r \rightarrow 0}{\simeq} -\frac{\lambda^4 m_\chi^2 (-m_L^4 + 3m_L^2 m_\chi^2 + m_\chi^4)}{96\pi (m_L^2 + m_\chi^2)^4} \quad (\text{A.4})$$

so the cross section is not s -wave suppressed.

Direct Detection: One loop diagrams of the form, Fig. 5 give rise to a charge radius, b_χ , and dipole moment, μ_χ .

$$b_\chi = \frac{e\lambda^2}{32\pi^2} \int_0^1 dw \left[\frac{((3w^3 - 3w^2 + 3w - 2)\bar{\Delta}_1 - (w-1)^3(w^2 m_\chi^2 - m_l^2))}{6\bar{\Delta}_1^2} - m_\chi^2 \frac{w^2(2w^2 - 3w + 1)}{3\bar{\Delta}_1^2} - \frac{w(w-1)}{2\bar{\Delta}_1} \right] \quad (\text{A.5})$$

and

$$\mu_\chi = \frac{e\lambda^2 m_\chi}{32\pi^2} \int_0^1 dw \left[-\frac{w(w-1)}{\bar{\Delta}_1} \right]. \quad (\text{A.6})$$

where

$$\bar{\Delta}_1 \equiv w(w-1)m_\chi^2 + (1-w)m_l^2 + w m_l^2. \quad (\text{A.7})$$

For the case of the electron partner, we replace m_e with 40 MeV since the minimum momentum transfer to the Xenon target at LUX is of this size, which cuts off the logarithmic divergence in the charge radius.

These lead to a scattering cross section from the charge radius interaction,

$$\frac{d\sigma_{b_\chi}}{dE_R} = \frac{m_N}{2\pi v^2} Z^2 e^2 b_\chi^2 F^2[E_R] \quad (\text{A.8})$$

and the magnetic dipole moment interaction,

$$\frac{d\sigma_{\text{DZ}}}{dE_R} = \frac{Z^2 e^2}{4\pi E_R} \mu_\chi^2 \left[1 - \frac{E_R}{v^2} \left(\frac{1}{2m_N} + \frac{1}{m_\chi} \right) \right] F^2[E_R] \quad (\text{A.9})$$

A.2 Complex Scalar Dark Matter

Relic Density:

$$a = \frac{\lambda^4 m_\chi^2 (1-r)^{3/2} r}{16\pi (m_L^2 - m_\chi^2 (r-1))^2} \quad (\text{A.10})$$

$$b = \frac{\lambda^4 m_\chi^2 \sqrt{1-r}}{384\pi (m_L^2 - m_\chi^2 (r-1))^4} \left[m_\chi^4 (r-1)^2 (9r^2 - 18r + 8) - 2m_L^2 m_\chi^2 (9r^3 - 31r^2 + 30r - 8) + m_L^4 (9r^2 - 2r + 8) \right] \quad (\text{A.11})$$

To lowest order in r we get,

$$a \stackrel{r \rightarrow 0}{\simeq} \frac{\lambda^4 m_\chi^2 r}{16\pi (m_L^2 + m_\chi^2)^2} \quad (\text{A.12})$$

$$b \stackrel{r \rightarrow 0}{\simeq} \frac{\lambda^4 m_\chi^2}{48\pi (m_L^2 + m_\chi^2)^2} \quad (\text{A.13})$$

exhibiting the chiral suppression of a .

Direct Detection: One loop diagrams of the form, Fig. 5 give rise to a charge radius, b_χ ,

$$b_\chi = \frac{e\lambda^2}{32\pi^2} \int_0^1 dw \left[\frac{w^3 (\overline{\Delta}_1 (6-4w) + w(m_\chi^2 (w-1)^2 + m_L^2))}{12\overline{\Delta}_1^2} - (m_L^2 \leftrightarrow m_l^2) \right]. \quad (\text{A.14})$$

where

$$\overline{\Delta}_1 \equiv w(w-1)m_\chi^2 + (1-w)m_l^2 + w m_l^2 \quad (\text{A.15})$$

Again, for the case of the electron partner, we replace m_e with 40 MeV since the log divergence is cut off by the minimum momentum transfer to the Xenon target. The charge radius scattering cross section is,

$$\frac{d\sigma_{b_\chi}}{dE_R} = \frac{m_N}{2\pi v^2} Z^2 e^2 b_\chi^2 F^2[E_R] \quad (\text{A.16})$$

A.3 Real Scalar Dark Matter

Relic Density:

$$a = \frac{m_\chi^2 (1-r)^{3/2} r \lambda^4}{4\pi (m_L^2 - m_\chi^2 (r-1))^2} \quad (\text{A.17})$$

$$b = \frac{m_\chi^2 \sqrt{1-r} r (9m_L^4 r + m_\chi^4 (r-1)^2 (-16+9r) - 2m_L^2 m_\chi^2 (16-25r+9r^2)) \lambda^4}{96\pi (m_L^2 - m_\chi^2 (r-1))^4} \quad (\text{A.18})$$

Both a and b vanish as $r \rightarrow 0$. To lowest order,

$$a \stackrel{r \rightarrow 0}{\simeq} r \frac{m_\chi^2 \lambda^4}{4\pi (m_L^2 + m_\chi^2)^2} \quad (\text{A.19})$$

$$b \stackrel{r \rightarrow 0}{\simeq} -r \frac{m_\chi^4 (2m_L^2 + m_\chi^2) \lambda^4}{6\pi (m_L^2 + m_\chi^2)^4} \quad (\text{A.20})$$

Direct Detection: The 2-loop contribution to the scattering cross section can be estimated using the effective operators from the relic density calculations. After integrating out L ,

$$\mathcal{L}_{eff} \sim \sum_l f_l m_l \chi^2 \bar{l} l \quad (\text{A.21})$$

where,

$$f_l = \frac{\lambda^2}{2(m_L^2 - m_\chi^2)}. \quad (\text{A.22})$$

Ref. [19] estimated the 2-loop contribution in the context of effective operators, from which we obtain

$$\frac{d\sigma}{dE_R} = \left(\frac{\alpha_{EM} Z}{2} \right)^4 \frac{E_R}{v^2} \left(\frac{2m_l^2 \lambda^4}{3\pi (m_L^2 - m_\chi^2)^2} \right) \tilde{F}(q) \quad (\text{A.23})$$

where $\tilde{F}(q)$ is the form factor for two photon scattering.

In comparison, $\frac{d\sigma}{dE_R}$ is $\mathcal{O}(10^8)$ times smaller for Real Scalar dark matter than for Dirac dark matter across the parameter space of interest, far below current experimental limits.

A.4 Majorana Dark Matter

Relic Density:

$$a = \frac{m_\chi^2 \sqrt{1-r} r \lambda^4}{32\pi (m_L^2 - m_\chi^2 (r-1))^2}, \quad (\text{A.24})$$

$$b = \frac{\lambda^4 m_\chi^2}{768\pi (m_L^2 - m_\chi^2 (r-1))^4 \sqrt{1-r}} \left[-2m_L^2 m_\chi^2 r (22 - 35r + 13r^2) + m_L^4 (16 - 26r + 13r^2) + m_\chi^4 (r-1)^2 (16 - 10r + 13r^2) \right] \quad (\text{A.25})$$

Thus, in the massless quark limit, the s -wave vanishes and we have the leading order results

$$a \stackrel{r \rightarrow 0}{\simeq} \frac{m_\chi^2 r \lambda^4}{32\pi(m_L^2 + m_\chi^2)^2} \quad (\text{A.26})$$

$$b \stackrel{r \rightarrow 0}{\simeq} \lambda^4 \frac{m_\chi^2 (m_L^4 + m_\chi^4)}{48\pi (m_L^2 + m_\chi^2)^4} \quad (\text{A.27})$$

Direct Detection: Following [26], the anapole moment for low 4-momentum transfer is given by

$$\mathcal{A} = -\frac{e\lambda^2}{96\pi^2 m_\chi^2} \left[\frac{3}{2} \log \frac{\mu}{\epsilon} - \frac{1 + 3\mu - 3\epsilon}{\sqrt{(\mu - 1 - \epsilon)^2 - 4\epsilon}} \operatorname{arctanh} \left(\frac{\sqrt{(\mu - 1 - \epsilon)^2 - 4\epsilon}}{\mu - 1 + \epsilon} \right) \right] \quad (\text{A.28})$$

where $\mu = \frac{m_L^2}{m_\chi^2}$ and $\epsilon = \frac{m_\ell^2}{m_\chi^2}$. When the 4-momentum transfer $|q^2|$ is comparable to the lepton mass as in the case of electron, the anapole moment is given by

$$\mathcal{A} = -\frac{e\lambda^2}{32\pi^2 m_\chi^2} \left[\frac{-10 + 12 \log \frac{\sqrt{|q^2|}}{m_\chi} - (3 + 9\mu) \log(\mu - 1) - (3 - 9\mu) \log \mu}{9(\mu - 1)} \right] \quad (\text{A.29})$$

Scattering due to anapole scattering is much larger than the 2-loop contribution. We compared to the LUX limits on the anapole moment derived in [26] and found that this was not a strong constraint on our parameter space even with the improvement expected for XENON1T.

References

- [1] S. Chang, R. Edezhath, J. Hutchinson, and M. Luty, “Effective WIMPs,” [arXiv:1307.8120 \[hep-ph\]](#).
- [2] H. An, L.-T. Wang, and H. Zhang, “Dark matter with t -channel mediator: a simple step beyond contact interaction,” [arXiv:1308.0592 \[hep-ph\]](#).
- [3] Y. Bai and J. Berger, “Fermion Portal Dark Matter,” *JHEP* **1311** (2013) 171, [arXiv:1308.0612 \[hep-ph\]](#).
- [4] A. DiFranzo, K. I. Nagao, A. Rajaraman, and T. M. P. Tait, “Simplified Models for Dark Matter Interacting with Quarks,” *JHEP* **1311** (2013) 014, [arXiv:1308.2679 \[hep-ph\]](#).

- [5] M. Papucci, A. Vichi, and K. M. Zurek, “Monojet versus rest of the world I: t-channel Models,” [arXiv:1402.2285 \[hep-ph\]](#).
- [6] O. Buchmuller, M. J. Dolan, and C. McCabe, “Beyond Effective Field Theory for Dark Matter Searches at the LHC,” *JHEP* **1401** (2014) 025, [arXiv:1308.6799 \[hep-ph\]](#).
- [7] H. An, R. Huo, and L.-T. Wang, “Searching for Low Mass Dark Portal at the LHC,” *Phys.Dark Univ.* **2** (2013) 50–57, [arXiv:1212.2221 \[hep-ph\]](#).
- [8] I. M. Shoemaker and L. Vecchi, “Unitarity and Monojet Bounds on Models for DAMA, CoGeNT, and CRESST-II,” *Phys.Rev.* **D86** (2012) 015023, [arXiv:1112.5457 \[hep-ph\]](#).
- [9] M. Cirelli, N. Fornengo, and A. Strumia, “Minimal dark matter,” *Nucl.Phys.* **B753** (2006) 178–194, [arXiv:hep-ph/0512090 \[hep-ph\]](#).
- [10] C. Cheung and D. Sanford, “Simplified Models of Mixed Dark Matter,” [arXiv:1311.5896 \[hep-ph\]](#).
- [11] **Planck** Collaboration, P. Ade *et al.*, “Planck 2013 results. XVI. Cosmological parameters,” [arXiv:1303.5076 \[astro-ph.CO\]](#).
- [12] **CMS Collaboration** Collaboration, S. Chatrchyan *et al.*, “Search for new physics in final states with a lepton and missing transverse energy in pp collisions at the LHC,” *Phys.Rev.* **D87** (2013) 072005, [arXiv:1302.2812 \[hep-ex\]](#).
- [13] “Search for direct-slepton and direct-chargino production in final states with two opposite-sign leptons, missing transverse momentum and no jets in 20/fb of pp collisions at $\sqrt{s} = 8$ TeV with the ATLAS detector,” Tech. Rep. ATLAS-CONF-2013-049, CERN, Geneva, May, 2013.
- [14] **CMS Collaboration** Collaboration, “Search for electroweak production of charginos, neutralinos, and sleptons using leptonic final states in pp collisions at 8 TeV,” Tech. Rep. CMS-PAS-SUS-13-006, CERN, Geneva, 2013.
- [15] J. Alwall, M. Herquet, F. Maltoni, O. Mattelaer, and T. Stelzer, “MadGraph 5 : Going Beyond,” *JHEP* **1106** (2011) 128, [arXiv:1106.0522 \[hep-ph\]](#).
- [16] N. D. Christensen and C. Duhr, “FeynRules - Feynman rules made easy,” *Comput.Phys.Commun.* **180** (2009) 1614–1641, [arXiv:0806.4194 \[hep-ph\]](#).

- [17] M. Pospelov and T. ter Veldhuis, “Direct and indirect limits on the electromagnetic form-factors of WIMPs,” *Phys.Lett.* **B480** (2000) 181–186, [arXiv:hep-ph/0003010](#) [hep-ph].
- [18] R. Bernabei, P. Belli, F. Montecchia, F. Nozzoli, F. Cappella, *et al.*, “Investigating electron interacting dark matter,” *Phys.Rev.* **D77** (2008) 023506, [arXiv:0712.0562](#) [astro-ph].
- [19] J. Kopp, V. Niro, T. Schwetz, and J. Zupan, “DAMA/LIBRA and leptonically interacting Dark Matter,” *Phys.Rev.* **D80** (2009) 083502, [arXiv:0907.3159](#) [hep-ph].
- [20] R. Essig, J. Mardon, and T. Volansky, “Direct Detection of Sub-GeV Dark Matter,” *Phys.Rev.* **D85** (2012) 076007, [arXiv:1108.5383](#) [hep-ph].
- [21] R. Essig, A. Manalaysay, J. Mardon, P. Sorensen, and T. Volansky, “First Direct Detection Limits on sub-GeV Dark Matter from XENON10,” *Phys.Rev.Lett.* **109** (2012) 021301, [arXiv:1206.2644](#) [astro-ph.CO].
- [22] P. Agrawal, S. Blanchet, Z. Chacko, and C. Kilic, “Flavored Dark Matter, and Its Implications for Direct Detection and Colliders,” *Phys.Rev.* **D86** (2012) 055002, [arXiv:1109.3516](#) [hep-ph].
- [23] B. Batell, T. Lin, and L.-T. Wang, “Flavored Dark Matter and R-Parity Violation,” [arXiv:1309.4462](#) [hep-ph].
- [24] **LUX Collaboration** Collaboration, D. Akerib *et al.*, “First results from the LUX dark matter experiment at the Sanford Underground Research Facility,” [arXiv:1310.8214](#) [astro-ph.CO].
- [25] DMtools. <http://dmtools.brown.edu/>.
- [26] J. Kopp, L. Michaels, and J. Smirnov, “Loopy Constraints on Leptophilic Dark Matter and Internal Bremsstrahlung,” [arXiv:1401.6457](#) [hep-ph].
- [27] A. Geringer-Sameth and S. M. Koushiappas, “Exclusion of canonical WIMPs by the joint analysis of Milky Way dwarfs with Fermi,” *Phys.Rev.Lett.* **107** (2011) 241303, [arXiv:1108.2914](#) [astro-ph.CO].
- [28] **Fermi-LAT collaboration** Collaboration, M. Ackermann *et al.*, “Constraining Dark Matter Models from a Combined Analysis of Milky Way Satellites with the Fermi Large Area Telescope,” *Phys.Rev.Lett.* **107** (2011) 241302, [arXiv:1108.3546](#) [astro-ph.HE].

- [29] T. Blum, A. Denig, I. Logashenko, E. de Rafael, B. Lee Roberts, *et al.*, “The Muon (g-2) Theory Value: Present and Future,” [arXiv:1311.2198 \[hep-ph\]](#).
- [30] S. P. Martin and J. D. Wells, “Muon anomalous magnetic dipole moment in supersymmetric theories,” *Phys.Rev.* **D64** (2001) 035003, [arXiv:hep-ph/0103067 \[hep-ph\]](#).
- [31] Y. Bai and J. Berger, “Lepton Portal Dark Matter,” [arXiv:1402.6696 \[hep-ph\]](#).